

Evolution of Stellar Activity and Habitable Zone II: Ca II H&K Emissions of Late-type Dwarfs

HENGGENG HAN ,¹ SONG WANG ,^{1,2,*} XUE LI ,³ CHUANJIE ZHENG ,³ JIAHUI WANG ,^{1,3} AND JIFENG LIU ,^{1,3,2,4}

¹*National Astronomical Observatories, Chinese Academy of Sciences, Beijing 100101, People's Republic of China*

²*Institute for Frontiers in Astronomy and Astrophysics, Beijing Normal University, Beijing, 102206, People's Republic of China*

³*School of Astronomy and Space Science, University of Chinese Academy of Sciences, Beijing 100049, People's Republic of China*

⁴*New Cornerstone Science Laboratory, National Astronomical Observatories, Chinese Academy of Sciences, Beijing, 100012, People's Republic of China*

ABSTRACT

Stellar chromospheric activity serves as a valuable proxy for estimating stellar ages, though its applicable range and accurate functional form are still debated. In this study, utilizing the LAMOST spectra we compiled a catalog of open cluster members and field stars to investigate R'_{HK} –age relations across various spectral types. We find that a linear model, specifically a Skumanich-type relation, can best describe the overall decline of chromospheric activity with age, with the slope varying across different spectral types. However, we also identify variations in the decay rate along the main sequence, which call for more accurate follow-up investigation. Finally, we find that lower-metallicity stars exhibit enhanced activity for F-, G-, and K-type stars, whereas no clear metallicity dependence is observed for M dwarfs.

Keywords: Late-type stars (909); Stellar activity (1580); Stellar ages (1581); Stellar rotation (1629)

1. INTRODUCTION

Late-type stars will spin down as they evolved due to the angular momentum loss caused by magnetized stellar winds (L. Mestel 1968; S. D. Kawaler 1988). As a result, stellar rotation periods can serve as a diagnostic of stellar ages, an approach known as gyrochronology (S. A. Barnes 2003). Given the close connection between magnetic activity and rotation, magnetic activity is therefore also expected to evolve with age.

One of the pioneering studies on the evolution of stellar magnetic activity was conducted by A. Skumanich (1972), who proposed an inverse square-root law relating magnetic activity, rotation and Li abundance to stellar age. Later on, some discrepancies appeared. For example, D. R. Soderblom et al. (1991) applied the Skumanich-type relation to samples from A. H. Vaughan & G. W. Preston (1980) and found a different exponent, which they suggested will result in an overpopulation of young stars with ages below 1 Gyr. Meanwhile, they proposed that a curve could also fit the data quite well, corresponding to a constant star formation rates.

As sample sizes continued to grow, increasing discrepancies with this simple picture continued to emerge.

On the one hand, some studies still supported the Skumanich-type scenario. D. Lorenzo-Oliveira et al. (2018) compiled an elite sample of solar twins and suggested the Skumanich-type relation may extend to ~ 6 Gyr, a finding further supported by L. Long et al. (2025) using open cluster members. Meanwhile, L. Ye et al. (2024) calibrated activity–age relations using *Kepler*–LAMOST overlap stars and proposed they remain valid for G- and K-type dwarfs up to ~ 13 Gyr.

Conversely, other studies argued that the evolutionary history was more complex. Some proposed an initial rapid decline in chromospheric activity followed by a phase in which activity level almost keeps unchanged (G. Pace & L. Pasquini 2004; G. Pace et al. 2009). Others have identified and modeled variable decay rates at different evolutionary stages (E. E. Mamajek & L. A. Hillenbrand 2008; R. S. Booth et al. 2017). These works suggested that the activity–age relations may present variable decay rate.

While activity–age relations have been extensively studied for open clusters, research on old field dwarfs has long been constrained by the lack of reliable age estimates for large samples. To systematically investigate the evolution of chromospheric activity across different stellar types and evolutionary phases, it is essential to combine both young open clusters and old field

* Corresponding author: songw@bao.ac.cn

stars. Recently J.-H. Wang et al. (2025) derived ages for ~ 4 million LAMOST DR10 dwarfs. This large field star sample, together with existing open cluster observations, now enables the extension and calibration of the activity–age relation across a vast age range, which may enable a more universally applicable relation.

In our series paper, X. Li et al. (2025) (hereafter Paper 1), we explored the activity–age relations for F-, G-, K-, and M-type dwarfs using near-ultraviolet observations. We showed that the magnetic activity evolution differs across spectral types and is also influenced by stellar metallicity. Building on that work, this paper combines the sample from Paper 1 with LAMOST spectra to conduct a systematic investigation of the evolution of Ca II H&K emissions in late-type stars. The paper is organized as follows. Section 2 describes our sample selection and the computation of chromospheric activity indices. In Section 3 we present our results. Finally, a discussion and a summary are given in Sections 4 and 5, respectively.

2. SAMPLE AND METHODS

2.1. Sample construction

2.1.1. Open Clusters

Members of open clusters exhibit similar stellar properties, making them well-suited for age determination via isochrone fitting. In Paper 1, we constructed a large sample of open cluster members with 1,573,928 targets, incorporating data from T. Cantat-Gaudin et al. (2020); M. Kounkel et al. (2020); C. J. Hao et al. (2022); A. Castro-Ginard et al. (2022); Z. He et al. (2023); E. L. Hunt & S. Reffert (2024). For a detailed description of this sample selection, we refer to Section 2.1 of Paper 1. This catalog was then cross-matched with the LAMOST Data Release 12 (DR12) to obtain low-resolution spectra.

2.1.2. Field stars

As established by previous studies, stellar chemical abundances serve as reliable indicators of stellar age (M. Haywood et al. 2013; M. Xiang et al. 2017). Recently, J.-H. Wang et al. (2025) constructed a training set of stars with well-determined ages, including wide binaries, field stars, and open cluster members, and applied the XGBoost machine learning algorithm to LAMOST spectra to derive ages for around 4 million late-type dwarfs. This extensive sample provides an excellent opportunity to study the evolution of chromospheric activity in late-type stars. For our work, we built a sample of field stars by cross-matching low-resolution spectra from LAMOST DR12 with this age catalog.

2.1.3. Stellar parameters

In this study, we retained only spectra with a signal-to-noise ratio (S/N) greater than 10 in the g band. Stellar parameters, including effective temperature (T_{eff}), surface gravity ($\log g$), and metallicity ($[\text{Fe}/\text{H}]$), were collected from LAMOST DR12 catalog, in which they were derived using the LAMOST Stellar Parameter Pipeline (LASP; A.-L. Luo et al. 2015). For stars with multiple observations, we selected the spectrum with the highest S/N. Meanwhile, we applied a cut of $\log g \geq 3.5$ to both the open cluster members and field stars to only keep dwarfs in our sample. Additionally, *Gaia* magnitudes, *renormalized unit weight error* (ruwe) values and distances were obtained from the *Gaia* early Data Release 3 (eDR3; Gaia Collaboration et al. 2021) and the catalog of C. A. L. Bailer-Jones et al. (2021), respectively. To ensure reliable distance measurements, we retained only stars located within 5 kpc and with relative parallax errors smaller than 0.2. Finally, to minimize contamination from binary systems, we excluded targets with ruwe exceeding 1.4.

The color excess values $E(B - V)$ were obtained from G. M. Green et al. (2019) and D. J. Schlegel et al. (1998), while interstellar extinction was calculated using the coefficients from E. L. Fitzpatrick (1999). In Paper 1, we categorized the sample into different subtypes based on their $(BP - RP)_0$ colors, then for each subtype we derived two typical ages to mark its entering and existing points of the main sequence with the MESA Isochrones and Stellar Tracks (B. Paxton et al. 2011; J. Choi et al. 2016; A. Dotter 2016). Following a similar approach, in this work we divided our sample into four types (F/G/K/M) according to their $(BP - RP)_0$ colors and excluded stars that have already left the main sequence by comparing their measured ages against the typical age values.

2.2. S -index and R'_{HK}

One of the most widely used proxies for chromospheric activity is the Ca II H&K emission, which at first were usually quantified using the well-known S –index based on the Mount Wilson observations (S_{MW}) (A. H. Vaughan et al. 1978). It was defined as the ratio of fluxes between the emission cores of Ca II H&K lines and the continua at both sides of the lines. However, this index still contains contribution from the photosphere. Later works then converted the S –index into pure chromospheric activity index R'_{HK} (F. Middelkoop 1982; R. W. Noyes et al. 1984).

It should be noted that there are multiple approaches to derive R'_{HK} from spectroscopic data (e.g., M. Mittag et al. 2013; N. Astudillo-Defru et al. 2017; S. Boro

Table 1. Stellar parameters, stellar activity indices, stellar ages of open cluster members.

ID	R.A. degree	Decl. degree	T_{eff} (K)	$\log g$ (dex)	[Fe/H] (dex)	Distance (pc)	$(B - V)_0$ (mag)	$(BP - RP)_0$ (mag)	S_{MW}	$\log_{10}(\text{Age})$	$\log_{10}(R'_{\text{HK}})$	S/N
(1)	(2)	(3)	(4)	(5)	(6)	(7)	(8)	(9)	(10)	(11)	(12)	(13)
43575746050631808	58.19351	17.10035	6040 \pm 66	4.19 \pm 0.1	-0.13 \pm 0.07	985 \pm 36	0.55	0.72	0.34 \pm 0.15	8.93	-4.38 \pm 0.27	24.58
45586099981415424	61.57953	16.61004	6155 \pm 60	4.23 \pm 0.09	-0.14 \pm 0.06	1426 \pm 63	0.53	0.76	0.48 \pm 0.18	8.93	-4.17 \pm 0.2	23.87
46167363676264320	60.42560	15.89299	5082 \pm 31	3.27 \pm 0.04	-0.71 \pm 0.03	920 \pm 20	0.88	0.99	0.22 \pm 0.05	8.93	-4.89 \pm 0.15	83.96
46230585594749824	60.82205	16.56147	6136 \pm 33	4.17 \pm 0.05	0.11 \pm 0.03	1060 \pm 32	0.53	0.79	0.18 \pm 0.08	8.93	-4.81 \pm 0.38	48.22
46347782365527936	61.64106	16.86522	5936 \pm 48	4.29 \pm 0.07	-0.25 \pm 0.05	762 \pm 16	0.58	0.76	0.23 \pm 0.07	8.93	-4.65 \pm 0.23	36.38
46471516080239232	59.75991	16.75634	4864 \pm 60	4.64 \pm 0.09	-0.33 \pm 0.06	1034 \pm 45	0.98	1.11	0.19 \pm 0.27	8.93	-5.04 \pm 0.71	24.68
46566761274958848	59.60302	17.16134	6178 \pm 28	4.22 \pm 0.04	-0.21 \pm 0.02	824 \pm 13	0.52	0.62	0.17 \pm 0.03	8.93	-4.85 \pm 0.15	130.38
46663690097339392	60.29038	17.47233	6044 \pm 73	4.28 \pm 0.11	-0.34 \pm 0.07	1096 \pm 41	0.55	0.76	0.29 \pm 0.25	8.93	-4.47 \pm 0.54	26.39
47804394753757056	64.05469	18.88450	3950 \pm 41	4.62 \pm 0.08	0.11 \pm 0.09	46 \pm 1	1.39	1.85	2.31 \pm 0.08	8.90	-4.55 \pm 0.02	135.35
48167955146062720	65.79015	19.20374	4117 \pm 35	4.61 \pm 0.05	-0.09 \pm 0.03	121 \pm 1	1.30	1.59	1.39 \pm 0.15	8.10	-4.64 \pm 0.05	50.33
...

(This table is available in its entirety in machine-readable form in the on line article.)

Table 2. Stellar parameters, stellar activity indices, stellar ages of field stars.

ID	R.A. degree	Decl. degree	T_{eff} (K)	$\log g$ (dex)	[Fe/H] (dex)	Distance (pc)	$(B - V)_0$ (mag)	$(BP - RP)_0$ (mag)	S_{MW}	$\log_{10}(\text{Age})$	$\log_{10}(R'_{\text{HK}})$	S/N
(1)	(2)	(3)	(4)	(5)	(6)	(7)	(8)	(9)	(10)	(11)	(12)	(13)
38655544960	45.00492	0.01991	4676 \pm 31	4.67 \pm 0.04	-0.18 \pm 0.03	314 \pm 2	1.07	1.21	0.52 \pm 0.1	9.59	-4.69 \pm 0.09	48.28
549755818112	45.04827	0.04831	4960 \pm 31	4.61 \pm 0.04	-0.26 \pm 0.03	615 \pm 11	0.93	1.13	0.33 \pm 0.09	9.82	-4.71 \pm 0.13	61.00
1275606125952	44.99326	0.07638	5452 \pm 74	4.46 \pm 0.12	-0.10 \pm 0.08	1476 \pm 110	0.75	0.9	0.27 \pm 0.26	9.87	-4.64 \pm 0.61	20.66
2920577765120	45.16461	0.15452	5810 \pm 69	4.29 \pm 0.11	-0.25 \pm 0.07	1563 \pm 86	0.63	0.8	0.11 \pm 0.2	9.82	-5.52 \pm 4.19	24.63
4230543624320	45.06346	0.19567	5971 \pm 67	4.22 \pm 0.11	0.18 \pm 0.07	1986 \pm 141	0.57	0.79	1.06 \pm 0.53	9.35	-3.79 \pm 0.24	10.02
6085969468928	44.92562	0.16888	5528 \pm 81	4.40 \pm 0.13	0.14 \pm 0.09	1816 \pm 155	0.71	0.88	0.09 \pm 0.20	9.83	-6.07 \pm 11.67	21.82
6223408420864	44.93745	0.18851	4783 \pm 37	4.62 \pm 0.05	-0.41 \pm 0.03	318 \pm 2	1.02	1.11	0.28 \pm 0.17	9.92	-4.91 \pm 0.30	42.56
6944962925824	44.97581	0.18788	5667 \pm 30	4.17 \pm 0.04	0.20 \pm 0.02	970 \pm 22	0.68	0.79	0.14 \pm 0.03	9.88	-5.14 \pm 0.28	101.20
8044474553216	44.92765	0.21918	5042 \pm 35	4.64 \pm 0.05	0.12 \pm 0.03	591 \pm 11	0.89	1.08	0.25 \pm 0.21	9.66	-4.82 \pm 0.44	38.35
9281425163264	45.16498	0.20028	6105 \pm 15	4.14 \pm 0.02	0.11 \pm 0.01	261 \pm 1	0.54	0.65	0.20 \pm 0.02	9.50	-4.74 \pm 0.09	210.62
...

(This table is available in its entirety in machine-readable form in the on line article.)

Saikia et al. 2018). Recent work by V. Perdelwitz et al. (2021) showed that during R'_{HK} calculation, direct Ca II H&K flux measurement (without S-index conversion) from observed spectra and using the synthetic spectra for photospheric rectification may yield more reliable results when the spectral resolution is high than \approx 20,000. Given that LAMOST spectra have a resolution of only $R \sim$ 1800, we used the classical method to convert S -index to R'_{HK} . We calculated the S -indices of LAMOST spectra (S_{LAMOST}) following the definition of A. H. Vaughan et al. (1978).

Furthermore, to convert the S_{LAMOST} into the pure chromospheric activity index R'_{HK} , an additional calibration between S_{LAMOST} and Mount Wilson S_{MW} is necessary. We adopted the calibration established by H. Han et al. (2025), which is valid for stars with $[\text{Fe}/\text{H}] > -1$. In brief, the authors simulated chromospheric activity by adding gaussian profiles to PHOENIX syn-

thetic spectra (T.-O. Husser et al. 2013), which were further convolved to different resolutions. Later on, relations between S_{SW} and S_{SPECTRUM} (e.g., S_{LAMOST}) corresponding to different resolutions have been established. Such conversion could minimize the influence of low spectral resolution. A detailed description of the calculation processes are given in H. Han et al. (2025). We adopted the methods of R. W. Noyes et al. (1984) and F. Middelkoop (1982) to calculate R'_{HK} :

$$R'_{\text{HK}} = 1.34 \times 10^{-4} \times C'_{\text{cf}} \times S_{\text{MW}} - R_{\text{phot}}. \quad (1)$$

Here R_{phot} is the photospheric contribution and C'_{cf} is the conversion factor. Both are functions of the stellar intrinsic color $(B - V)_0$, which were calculated by interpolating the T_{eff} using the results from M. J. Pecaut & E. E. Mamajek (2013).

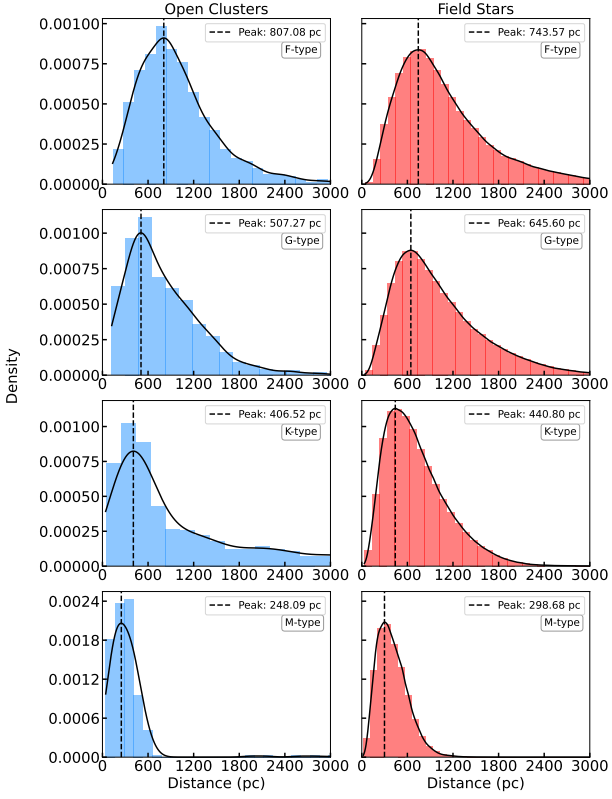


Figure 1. Histograms of distances corresponding to open cluster members and field stars across various stellar types. Peak positions are marked using black dashed lines.

3. RESULTS

In this work, we combined both open cluster members and field stars to investigate the evolution of chromospheric activity across different evolutionary stages. We listed all our targets together with stellar parameters, activity indices and ages in Table 1 and Table 2. In total we got 5,748 open cluster members and 1,674,191 field stars. We divided our sample into subgroups according to their T_{eff} . For F-type, G-type, K-type, and M-type dwarfs we adopted $6,000 \text{ K} \leq T_{\text{eff}} < 6,500 \text{ K}$, $5,300 \text{ K} < T_{\text{eff}} \leq 6,000 \text{ K}$, $4,000 \text{ K} < T_{\text{eff}} \leq 5,300 \text{ K}$, and $3,800 \text{ K} < T_{\text{eff}} \leq 4,000 \text{ K}$, respectively. For each subgroup, we retained only targets with distances smaller than the peak of the distance histogram specific to that subgroup, ensuring a volume-complete sample. This completeness cut was applied separately to the open clusters and field stars (Figure 1).

Following the results of J.-H. Wang et al. (2025), To ensure reliable age estimation, we restricted our analysis of field stars to those with spectra having a S/N greater than 20 and ages between 1 and 10 Gyr. In contrast, for the open cluster sample, given the limited number of sample older than 1 Gyr, we only focused on target

younger than 1 Gyr. To ensure reliable measurements of R'_{HK} , we further limited our sample to stars with activity levels in the range $10^{-5.5} \leq R'_{\text{HK}} \leq 10^{-3}$. Meanwhile, for each spectral subtype we binned the data along the age axis and computed the median trend (Figure 2). For both open cluster members and field stars, the observed age range was divided into ten bins in the log space. Within each bin, the median $\log_{10}(R'_{\text{HK}})$ value was taken as the representative activity level, and the associated uncertainty was estimated from the scatter of the data (i.e., standard deviation) in that bin.

Besides the classical Skumanich-type relation, polynomial with different degrees have been carried out to model the evolution of stellar activity (e.g. E. E. Mamajek & L. A. Hillenbrand 2008; J. Zhang et al. 2019). In this work, we applied 1st-, 2nd-, and 3-rd degree polynomial:

$$\log_{10}(R'_{\text{HK}}) = \sum_{i=0}^n a_i (\log_{10} t)^{n-i}, \quad n = 1, 2, 3 \quad (2)$$

to fit the R'_{HK} –age relation. Here t is stellar age.

We performed Bayesian model comparison using the *dynesty* package (J. S. Speagle 2020; S. Koposov et al. 2025), which implements nested sampling (J. Skilling 2004; J. Skilling 2006). We used dynamic nested sampling (E. Higson et al. 2019) with multi-ellipsoid bounding (F. Feroz et al. 2009) and random walk (J. Skilling 2006). The maximum a posteriori (MAP) estimation was obtained by selecting the sample with the highest likelihood from the resampled posterior distribution, which we adopted as our best-fit solution. The uncertainties of the *evidence* were estimated following N. Chopin & C. Robert (2008); E. Higson et al. (2018); J. S. Speagle (2020). Uniform priors were applied to all model parameters. The likelihood function was written as:

$$\ln [p(y | x, \sigma, \mathbf{a})] = -\frac{1}{2} \sum_n \frac{\left[y_n - \sum_{i=0}^{n_{\text{deg}}} a_i x_n^{n_{\text{deg}}-i} \right]^2}{\sigma_n^2} - \frac{1}{2} \sum_n \ln(2\pi\sigma_n^2), \quad (3)$$

Here y is observed chromospheric activity level, x is stellar age, and σ is the uncertainty of R'_{HK} . The polynomial models were constrained to be monotonically decreasing. Examples of the resulting posterior corner plots are shown in Figure A2. The fitting results are summarized in Table 3. Figure 2 shows all the activity–age relations for different types of stars.

In addition, to test whether the error of R'_{HK} in each age bin is reasonable (and has no significant impact on

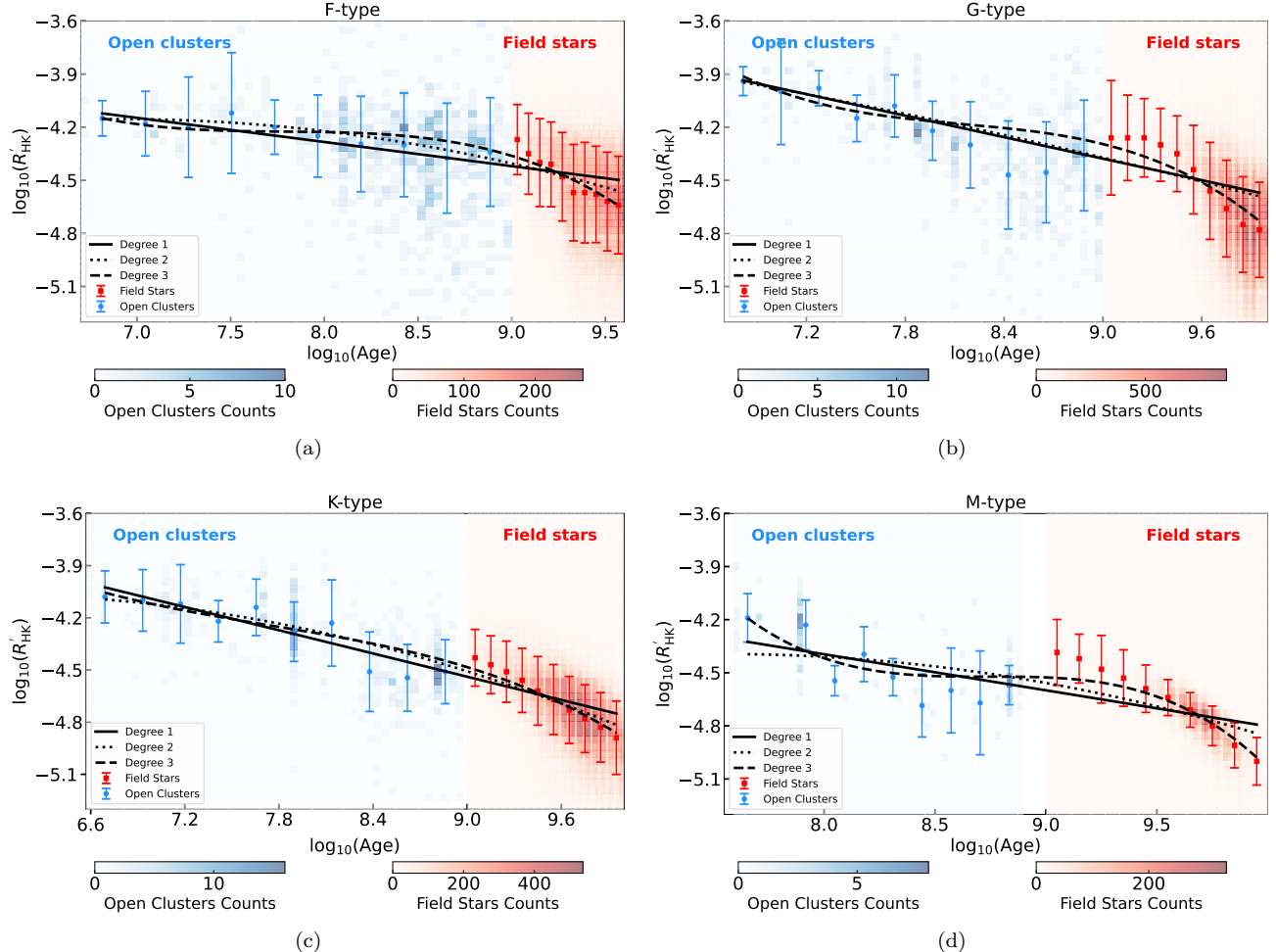


Figure 2. R'_HK –age relations of different kinds of stars. Panel (a), (b), (c), and (d) represents F-, G-, K-, and M-type dwarfs, respectively. Members of open clusters are presented in blue while field stars are presented in red. Blue and red dots with errorbars are binned median points. Black lines are best-fit models corresponding to maximum a posteriori.

the fit), we applied an alternative fit for the G-type stars (as an example), in which the uncertainty of R'_HK was set as a free parameter. The likelihood function was written as:

$$\ln [p(y | x, \sigma, a)] = -\frac{1}{2} \sum_n \frac{\left[y_n - \sum_{i=0}^{n_{\text{deg}}} a_i x_n^{n_{\text{deg}}-i} \right]^2}{\sigma^2} - \frac{1}{2} \sum_n \ln(2\pi\sigma^2). \quad (4)$$

The fitting results (Figure A2 and A3) show that the derived uncertainty is smaller than the standard deviation of $\log_{10}(R'_\text{HK})$ in each bin, yet the fitted activity–age relations remain similar. We therefore concluded that using the standard deviation of $\log_{10}(R'_\text{HK})$ in each bin as the error is a robust choice for the fitting.

4. DISCUSSIONS

4.1. Chromospheric activity–age relations

The long-term evolution of chromospheric activity has been studied extensively. Early studies primarily focused on members of open clusters, whose ages can be reliably estimated via isochrone fitting. The classical framework was established by A. Skumanich (1972), who modeled this evolution using a power-law relation (i.e., a linear function in log–log space). In this paradigm, chromospheric activity levels can serve as effective age indicators. The Skumanich-law was not only observed in activity proxies but also in strength of magnetic field for both pre-main sequence stars and main sequence stars (A. A. Vidotto et al. 2014).

Early studies on the evolution of chromospheric activity primarily focused on open cluster members. Several works have suggested that chromospheric activity declines rapidly and reaches a minimum on a relatively

Table 3. Best-fit parameters and their asymmetric uncertainties for various models.

Type	Degree	a_3	a_2	a_1	a_0	$\Delta \ln Z_3$	$\Delta \ln Z_2$
F	3rd	32.406864 (+7.810729) (-32.33927)	-14.106963 (+12.545303) (-2.483614)	1.8111 (+0.263676) (-1.61206)	-0.077505 (+0.068663) (-0.009086)	-	-
	2nd	0	-6.895304 (+4.85691) (-0.555807)	0.793518 (+0.117668) (-1.206769)	-0.057422 (+0.074243) (-0.005558)	8.26 ± 0.21	-
	1st	0	0	-3.192104 (+0.385153) (-0.376219)	-0.136439 (+0.045864) (-0.047042)	16.28 ± 0.19	8.02 ± 0.18
G	3rd	30.672866 (+16.415716) (-26.186224)	-12.65184 (+9.733918) (-5.997482)	1.541196 (+0.725148) (-1.191598)	-0.063014 (+0.048519) (-0.029119)	-	-
	2nd	0	-3.300006 (+2.750964) (-2.500602)	-0.018874 (+0.614954) (-0.675009)	-0.011136 (+0.041134) (-0.037133)	7.73 ± 0.21	-
	1st	0	0	-2.556173 (+0.300929) (-0.316545)	-0.202412 (+0.039553) (-0.037614)	15.5 ± 0.19	7.77 ± 0.18
K	3rd	11.88574 (+26.852062) (-13.338222)	-5.912632 (+5.012869) (-9.749875)	0.738307 (+1.173542) (-0.625596)	-0.031492 (+0.025862) (-0.046964)	-	-
	2nd	0	-5.70103 (+3.986852) (-0.730112)	0.550257 (+0.184412) (-0.973174)	-0.04641 (+0.058596) (-0.011497)	7.46 ± 0.2	-
	1st	0	0	-2.535415 (+0.322496) (-0.33898)	-0.222606 (+0.039595) (-0.037625)	15.75 ± 0.19	8.29 ± 0.18
M	3rd	171.556481 (+10.846179) (-78.643357)	-60.482639 (+26.873159) (-3.393348)	6.925193 (+0.349516) (-3.055421)	-0.264304 (+0.115555) (-0.011793)	-	-
	2nd	0	-8.83914 (+7.515438) (-0.041887)	1.177009 (+0.021025) (-1.712276)	-0.077924 (+0.096533) (-0.001855)	3.37 ± 0.21	-
	1st	0	0	-2.765918 (+0.362286) (-0.364146)	-0.203693 (+0.040981) (-0.040461)	11.25 ± 0.2	7.88 ± 0.18

Note: $\Delta \ln Z_j = \ln Z_{\text{current row model}} - \ln Z_{\text{model } j}$. Positive values indicate the current model is favored over model j , where j denotes the polynomial degree. Uncertainties for coefficients are shown in parentheses in the row below each model.

short timescale. For example, [G. Pace & L. Pasquini \(2004\)](#) and [G. Pace et al. \(2009\)](#) proposed very similar timescales of approximately 1.5 Gyr and 1.2 Gyr, respectively. Later on, by incorporating field stars into the analysis, [G. Pace \(2013\)](#) found a “L-shape” model for chromospheric activity evolution, featuring a knee point at around 2 Gyr, beyond which the activity level will reach its minimum and remain nearly unchanged.

However, alternative perspectives have emerged from other studies. [E. E. Mamajek & L. A. Hillenbrand \(2008\)](#) combined activity–rotation relations with gyrochronology to calibrate the activity–age relation for F7–K2 dwarfs aged between 0.6 and 4.5 Gyr. Later on, [D. Lorenzo-Oliveira et al. \(2018\)](#) derived Skumanich-type activity–age relation for solar twins using HARPS spectra, with stellar ages determined through isochrone fitting. They argued that chromospheric activity remains a valid age indicator for stars up to 7 Gyr. More recent works have further highlighted the necessity of accounting for stellar mass and metallicity when con-

structing activity–age relations (e.g., [P. V. Souza dos Santos et al. 2024](#); [G. Carvalho-Silva et al. 2025](#)).

Given that first-, second-, and third-order polynomial models have all been proposed in earlier studies (e.g., [E. E. Mamajek & L. A. Hillenbrand 2008](#); [D. Lorenzo-Oliveira et al. 2018](#); [J. Zhang et al. 2019](#); [L. Long et al. 2025](#)) to describe magnetic activity evolution, our large sample provides a robust opportunity to assess which of these models offers the best description of the data. In Section 3, we explored various models to describe the activity–age relation. We computed the Bayesian evidence ($\ln Z$) for each model using the *dynesty* Python package ([J. S. Speagle 2020](#); [S. Koposov et al. 2025](#)) and applied Jeffreys’ scale ($\Delta \ln Z$) to judge which model is better (See [R. Handberg & T. L. Campante \(2011\)](#) and reference in it for more details). Our analysis suggests that, across all spectral types, a simple linear model best describes the activity–age relation, although with different slopes.

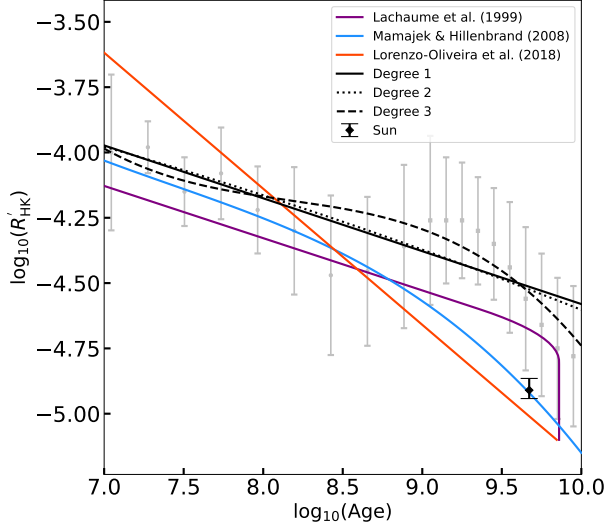


Figure 3. Comparisons of R'_HK –age relations for G-type stars from different works. Gray dots with errorbars are our G-type star sample. Black lines represent results from our work with different models. Purple, dodgerblue, and orange-red line shows the relation from R. Lachaume et al. (1999), E. E. Mamajek & L. A. Hillenbrand (2008), and D. Lorenzo-Oliveira et al. (2018), respectively. The Sun was shown as black diamond with the $R'_{\text{HK},\text{Sun}} = -4.91$ and its uncertainties adopted from E. E. Mamajek & L. A. Hillenbrand (2008).

However, we noted that the activity–age relation exhibits some features beyond a simple linear decline. After reaching the main sequence, chromospheric activity undergoes a relatively slow decay over a substantial timescale, a trend also reported by E. L. Shkolnik & T. S. Barman (2014) and T. Richey-Yowell et al. (2023) based on X-ray and ultraviolet observations. Both studies, as well as our analysis of field stars, reveal an abrupt drop in activity around ~ 1 Gyr. This transition is further supported by R. S. Booth et al. (2017), who detected a similar sharp decline using X-ray data from the *Chandra* and *XMM-Newton* satellites. The preference for a linear relation in this work may be driven by the large errors in the data points (Figure 2). This makes it difficult to determine whether these features are physically real, and consequently whether a higher-order polynomial is genuinely required to describe the activity evolution. Figure 3 compares our R'_HK –age relation of G dwarfs with those of previous works (R. Lachaume et al. 1999; E. E. Mamajek & L. A. Hillenbrand 2008; D. Lorenzo-Oliveira et al. 2018). The systematic offset in absolute R'_HK levels likely arises from differences in the calculation methods, whereas the differing evolutionary slopes may be attributed to different stellar samples used. Given the considerable uncertainties in the data,

it remains difficult to judge which model provides a more accurate description of the activity evolution.

Recent studies have proposed a complex evolution behavior of stellar rotation. For example, core-envelope coupling (e.g. F. Gallet & J. Bouvier 2013; F. Spada & A. C. Lanzaflame 2020) and weakened magnetic braking (J. L. van Saders et al. 2016) can redistribute stellar angular momentum, which will influence stellar activity levels. As a result, the relation between chromospheric activity and stellar rotation period will evolve with time. This behavior may result in non-uniform decay rate in the activity–rotation relation, which have been observed by some recent researches.

For example, H. Yang et al. (2025) suggested a four-segment activity–rotation relation, connecting it to three phases of gyrochronology and one weakened magnetic braking stage. Later on, H. Han et al. (2025) derived a new activity–rotation relation for M dwarfs and divided the intermediate region (corresponding to the “Gap” region of gyrochronology) into two parts with varying activity decay rate, indicating a change in the core-envelope coupling efficiency. These features suggest a varying relationship between activity and age during long-term stellar evolution. The complex behavior of activity–rotation relation is indicative of a non-uniform decay rate of chromospheric activity throughout stellar lives. More observations are needed to shed light on such issue.

The Sun exhibits $\log_{10}(R'_\text{HK})$ value in the range -4.942 – -4.865 (E. E. Mamajek & L. A. Hillenbrand 2008), much lower than that predicted by our new relation. To address whether the Sun is truly special, we compared its R'_HK value with those of solar twins in our sample, defined as stars with $5,677 \text{ K} \leq T_{\text{eff}} \leq 5,877 \text{ K}$, $4.2 \leq \log g \leq 4.6$, and $-0.2 \leq [\text{Fe}/\text{H}] \leq 0.2$ (Figure 4). The data clearly show that the chromospheric activity declines with stellar age. Although the Sun indeed lies among the least active stars, many solar twins exhibit activity levels comparable to the present-day Sun.

4.2. Influence of metallicity

Several studies have explored the potential influence of metallicity on R'_HK –age relations (e.g. W. Lyra & G. F. Porto de Mello 2005; D. Lorenzo-Oliveira et al. 2016; P. V. Souza dos Santos et al. 2024; G. Carvalho-Silva et al. 2025). In this work, we also examined how metallicity affects chromospheric activity. Given the limited number of stars in open clusters, our analysis focuses exclusively on field stars. In Figure 5, we show median R'_HK –age trends for different spectral types, with distinct colors representing different metallicity ranges. Overall, the decay rates of activity with age are similar

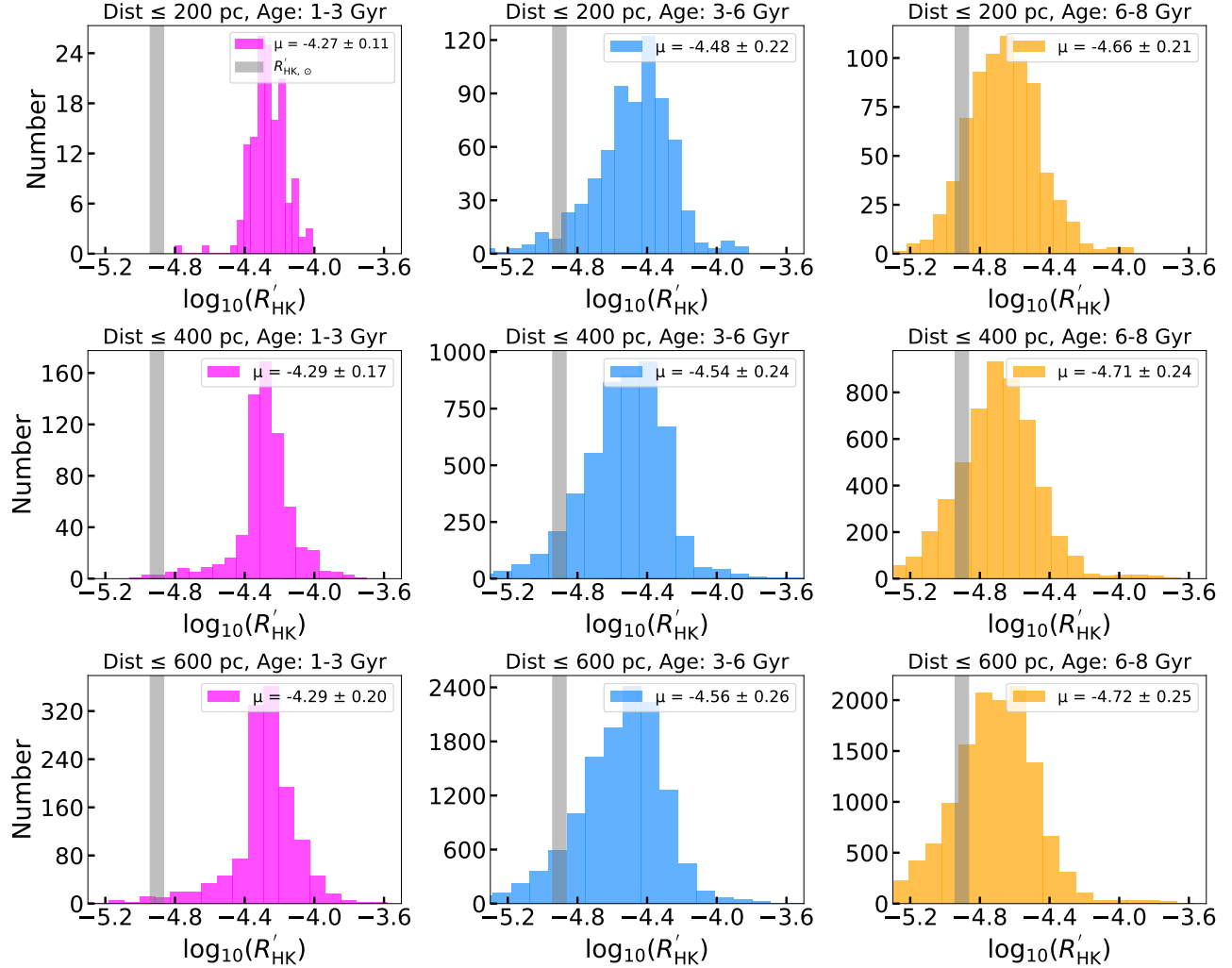


Figure 4. Histograms of $\log_{10}(R'_\text{HK})$ of solar twins. Different panels represent different age and distance ranges. Shaded areas mark the solar $\log_{10}(R'_\text{HK})$ range adopted from E. E. Mamajek & L. A. Hillenbrand (2008).

across different metallicity ranges, although systematic offsets in R'_HK are evident: metal-poor stars tend to exhibit higher R'_HK levels. Such metallicity stratification has also been revealed and calibrated by (G. Carvalho-Silva et al. 2025) and H. J. Rocha-Pinto & W. J. Maciel (1998).

Such phenomenon is likely due to the intrinsically shallower Ca II H&K absorption lines for metal-poor stars, which would lead to an apparent enhancement in measured activity (D. R. Soderblom et al. 1991). We noticed that such phenomenon is not obvious for young G-type dwarfs, which may be attributed to the limited number of stars in this region. In addition, this metallicity-dependent effect disappears for M dwarfs. In these cool stars, the Ca II H&K lines lack the broad wings seen in hotter stars because the dominant ionization stage is Ca I rather than Ca II that produces the broad wings (J. L. Linsky 2017). Strong TiO molecular

bands in M-dwarf spectra can obscure the shallow Ca II H&K absorption lines, making the influence of metallicity observationally indistinguishable.

5. SUMMARY

Although stellar chromospheric activity serves as an effective tracer of stellar ages, previous studies have employed a variety of models, mostly first-, second-, or third-degree polynomials, to describe this relation. In this work, we systematically examine the chromospheric activity–age relation across different stellar types by using a large combined sample of stars from open clusters and the field. The LAMOST spectroscopic data are used to calculate the chromospheric activity indices.

We model the activity–age relation using first-, second-, and third-degree polynomials, compute the Bayesian *evidence* for each model, and apply Jeffreys' scale to select the most appropriate model. Our anal-

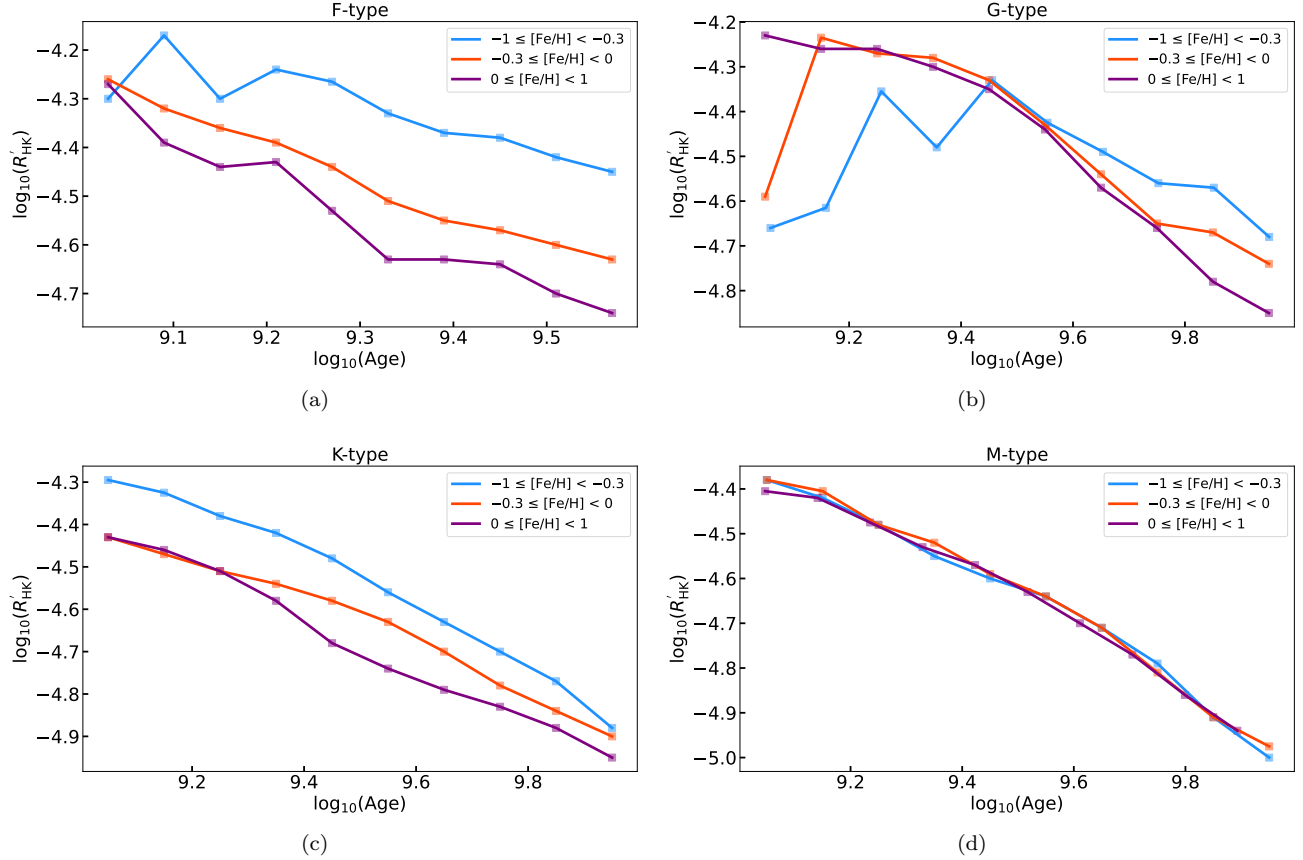


Figure 5. Median curves of R'_{HK} –age plane corresponding to different stellar types for field stars. Different colors represent different metallicity ranges.

ysis indicates that a linear (Skumanich-type) relation between $\log_{10}(R'_{\text{HK}})$ and $\log_{10}(\text{Age})$ provides a best description of how stellar chromospheric activity declines with age, with the slope varying across different spectral types. However, we also observe variations in the decay rate of chromospheric activity with age, which require more accurate follow-up investigation. In addition, although the Sun itself is among the least active stars, many solar twins exhibit activity levels similar to that of the present-day Sun. Finally, our results show that lower-metallicity stars exhibit enhanced activity for F-, G-, and K-type stars, consistent with weaker Ca II H&K absorption. However, no clear metallicity dependence is observed for M dwarfs, since their strong TiO molecular bands will overwhelm the already quite faint Ca II H&K absorption.

ACKNOWLEDGEMENTS

We thank the referee for the comprehensive comments and suggestions, which have greatly improved

this manuscript. The Guoshoujing Telescope (the Large Sky Area Multi-Object Fiber Spectroscopic Telescope LAMOST) is a National Major Scientific Project built by the Chinese Academy of Sciences. Funding for the project has been provided by the National Development and Reform Commission. LAMOST is operated and managed by the National Astronomical Observatories, Chinese Academy of Sciences. This work was supported by National Natural Science Foundation of China (NSFC) under grant Nos. 12588202/12273057/11833002/12090042, the National Key Research and Development Program of China (NKRDPC) under grant number 2023YFA1607901, the Strategic Priority Program of the Chinese Academy of Sciences under grant number XDB1160302, and science research grants from the China Manned Space Project. J.F.L acknowledges the support from the New Cornerstone Science Foundation through the New Cornerstone Investigator Program and the XPLORER PRIZE.

REFERENCES

Astudillo-Defru, N., Delfosse, X., Bonfils, X., et al. 2017, *A&A*, 600, A13, doi: [10.1051/0004-6361/201527078](https://doi.org/10.1051/0004-6361/201527078)

Bailer-Jones, C. A. L., Rybizki, J., Fouesneau, M., Demleitner, M., & Andrae, R. 2021, *AJ*, 161, 147, doi: [10.3847/1538-3881/abd806](https://doi.org/10.3847/1538-3881/abd806)

Barnes, S. A. 2003, *ApJ*, 586, 464, doi: [10.1086/367639](https://doi.org/10.1086/367639)

Booth, R. S., Poppenhaeger, K., Watson, C. A., Silva Aguirre, V., & Wolk, S. J. 2017, *MNRAS*, 471, 1012, doi: [10.1093/mnras/stx1630](https://doi.org/10.1093/mnras/stx1630)

Boro Saikia, S., Marvin, C. J., Jeffers, S. V., et al. 2018, *A&A*, 616, A108, doi: [10.1051/0004-6361/201629518](https://doi.org/10.1051/0004-6361/201629518)

Cantat-Gaudin, T., Anders, F., Castro-Ginard, A., et al. 2020, *A&A*, 640, A1, doi: [10.1051/0004-6361/202038192](https://doi.org/10.1051/0004-6361/202038192)

Carvalho-Silva, G., Meléndez, J., Rathsam, A., et al. 2025, *ApJL*, 983, L31, doi: [10.3847/2041-8213/adc382](https://doi.org/10.3847/2041-8213/adc382)

Castro-Ginard, A., Jordi, C., Luri, X., et al. 2022, *A&A*, 661, A118, doi: [10.1051/0004-6361/202142568](https://doi.org/10.1051/0004-6361/202142568)

Choi, J., Dotter, A., Conroy, C., et al. 2016, *ApJ*, 823, 102, doi: [10.3847/0004-637X/823/2/102](https://doi.org/10.3847/0004-637X/823/2/102)

Chopin, N., & Robert, C. 2008, arXiv e-prints, arXiv:0801.3887, doi: [10.48550/arXiv.0801.3887](https://doi.org/10.48550/arXiv.0801.3887)

Dotter, A. 2016, *ApJS*, 222, 8, doi: [10.3847/0067-0049/222/1/8](https://doi.org/10.3847/0067-0049/222/1/8)

Feroz, F., Hobson, M. P., & Bridges, M. 2009, *MNRAS*, 398, 1601, doi: [10.1111/j.1365-2966.2009.14548.x](https://doi.org/10.1111/j.1365-2966.2009.14548.x)

Fitzpatrick, E. L. 1999, *PASP*, 111, 63, doi: [10.1086/316293](https://doi.org/10.1086/316293)

Gaia Collaboration, Brown, A. G. A., Vallenari, A., et al. 2021, *A&A*, 649, A1, doi: [10.1051/0004-6361/202039657](https://doi.org/10.1051/0004-6361/202039657)

Gallet, F., & Bouvier, J. 2013, *A&A*, 556, A36, doi: [10.1051/0004-6361/201321302](https://doi.org/10.1051/0004-6361/201321302)

Green, G. M., Schlafly, E., Zucker, C., Speagle, J. S., & Finkbeiner, D. 2019, *ApJ*, 887, 93, doi: [10.3847/1538-4357/ab5362](https://doi.org/10.3847/1538-4357/ab5362)

Han, H., Wang, S., Li, X., Zheng, C., & Liu, J. 2025, *ApJ*, 984, 2, doi: [10.3847/1538-4357/adc600](https://doi.org/10.3847/1538-4357/adc600)

Han, H., Wang, S., Yang, H., et al. 2025, Varying core-envelope coupling efficiency identified from stellar rotation–activity relation, <https://arxiv.org/abs/2512.11376>

Handberg, R., & Campante, T. L. 2011, *A&A*, 527, A56, doi: [10.1051/0004-6361/201015451](https://doi.org/10.1051/0004-6361/201015451)

Hao, C. J., Xu, Y., Wu, Z. Y., et al. 2022, *A&A*, 660, A4, doi: [10.1051/0004-6361/202243091](https://doi.org/10.1051/0004-6361/202243091)

Haywood, M., Di Matteo, P., Lehnert, M. D., Katz, D., & Gómez, A. 2013, *A&A*, 560, A109, doi: [10.1051/0004-6361/201321397](https://doi.org/10.1051/0004-6361/201321397)

He, Z., Liu, X., Luo, Y., Wang, K., & Jiang, Q. 2023, *ApJS*, 264, 8, doi: [10.3847/1538-4365/ac9af8](https://doi.org/10.3847/1538-4365/ac9af8)

Higson, E., Handley, W., Hobson, M., & Lasenby, A. 2018, *Bayesian Analysis*, 13, 873, doi: [10.1214/17-BA1075](https://doi.org/10.1214/17-BA1075)

Higson, E., Handley, W., Hobson, M., & Lasenby, A. 2019, *Statistics and Computing*, 29, 891, doi: [10.1007/s11222-018-9844-0](https://doi.org/10.1007/s11222-018-9844-0)

Hunt, E. L., & Reffert, S. 2024, *A&A*, 686, A42, doi: [10.1051/0004-6361/202348662](https://doi.org/10.1051/0004-6361/202348662)

Husser, T.-O., Wende-von Berg, S., Dreizler, S., et al. 2013, *A&A*, 553, A6, doi: [10.1051/0004-6361/201219058](https://doi.org/10.1051/0004-6361/201219058)

Kawaler, S. D. 1988, *ApJ*, 333, 236, doi: [10.1086/166740](https://doi.org/10.1086/166740)

Koposov, S., Speagle, J., Barbary, K., et al. 2025, *joshspeagle/dynesty: v3.0.0, v3.0.0* Zenodo, doi: [10.5281/zenodo.17268284](https://doi.org/10.5281/zenodo.17268284)

Kounkel, M., Covey, K., & Stassun, K. G. 2020, *AJ*, 160, 279, doi: [10.3847/1538-3881/abc0e6](https://doi.org/10.3847/1538-3881/abc0e6)

Lachaume, R., Dominik, C., Lanz, T., & Habing, H. J. 1999, *A&A*, 348, 897

Li, X., Wang, S., Ma, J., et al. 2025, *ApJS*, 281, 13, doi: [10.3847/1538-4365/ae08a9](https://doi.org/10.3847/1538-4365/ae08a9)

Linsky, J. L. 2017, *ARA&A*, 55, 159, doi: [10.1146/annurev-astro-091916-055327](https://doi.org/10.1146/annurev-astro-091916-055327)

Long, L., Bi, S., Ye, L., et al. 2025, *MNRAS*, 542, 2431, doi: [10.1093/mnras/staf1335](https://doi.org/10.1093/mnras/staf1335)

Lorenzo-Oliveira, D., Porto de Mello, G. F., & Schiavon, R. P. 2016, *A&A*, 594, L3, doi: [10.1051/0004-6361/201629233](https://doi.org/10.1051/0004-6361/201629233)

Lorenzo-Oliveira, D., Freitas, F. C., Meléndez, J., et al. 2018, *A&A*, 619, A73, doi: [10.1051/0004-6361/201629294](https://doi.org/10.1051/0004-6361/201629294)

Luo, A.-L., Zhao, Y.-H., Zhao, G., et al. 2015, *Research in Astronomy and Astrophysics*, 15, 1095, doi: [10.1088/1674-4527/15/8/002](https://doi.org/10.1088/1674-4527/15/8/002)

Lyra, W., & Porto de Mello, G. F. 2005, *A&A*, 431, 329, doi: [10.1051/0004-6361:20040249](https://doi.org/10.1051/0004-6361:20040249)

Mamajek, E. E., & Hillenbrand, L. A. 2008, *ApJ*, 687, 1264, doi: [10.1086/591785](https://doi.org/10.1086/591785)

Mestel, L. 1968, *MNRAS*, 138, 359, doi: [10.1093/mnras/138.3.359](https://doi.org/10.1093/mnras/138.3.359)

Middelkoop, F. 1982, *A&A*, 107, 31

Mittag, M., Schmitt, J. H. M. M., & Schröder, K.-P. 2013, *A&A*, 549, A117, doi: [10.1051/0004-6361/201219868](https://doi.org/10.1051/0004-6361/201219868)

Noyes, R. W., Hartmann, L. W., Baliunas, S. L., Duncan, D. K., & Vaughan, A. H. 1984, *ApJ*, 279, 763, doi: [10.1086/161945](https://doi.org/10.1086/161945)

Pace, G. 2013, *A&A*, 551, L8, doi: [10.1051/0004-6361/201220364](https://doi.org/10.1051/0004-6361/201220364)

Pace, G., Meléndez, J., Pasquini, L., et al. 2009, *A&A*, 499, L9, doi: [10.1051/0004-6361/200912090](https://doi.org/10.1051/0004-6361/200912090)

Pace, G., & Pasquini, L. 2004, *A&A*, 426, 1021, doi: [10.1051/0004-6361:20040568](https://doi.org/10.1051/0004-6361:20040568)

Paxton, B., Bildsten, L., Dotter, A., et al. 2011, ApJS, 192, 3, doi: [10.1088/0067-0049/192/1/3](https://doi.org/10.1088/0067-0049/192/1/3)

Pecaut, M. J., & Mamajek, E. E. 2013, ApJS, 208, 9, doi: [10.1088/0067-0049/208/1/9](https://doi.org/10.1088/0067-0049/208/1/9)

Perdelwitz, V., Mittag, M., Tal-Or, L., et al. 2021, A&A, 652, A116, doi: [10.1051/0004-6361/202140889](https://doi.org/10.1051/0004-6361/202140889)

Richey-Yowell, T., Shkolnik, E. L., Schneider, A. C., et al. 2023, ApJ, 951, 44, doi: [10.3847/1538-4357/acd2dc](https://doi.org/10.3847/1538-4357/acd2dc)

Rocha-Pinto, H. J., & Maciel, W. J. 1998, MNRAS, 298, 332, doi: [10.1046/j.1365-8711.1998.01597.x](https://doi.org/10.1046/j.1365-8711.1998.01597.x)

Schlegel, D. J., Finkbeiner, D. P., & Davis, M. 1998, ApJ, 500, 525, doi: [10.1086/305772](https://doi.org/10.1086/305772)

Shkolnik, E. L., & Barman, T. S. 2014, AJ, 148, 64, doi: [10.1088/0004-6256/148/4/64](https://doi.org/10.1088/0004-6256/148/4/64)

Skilling, J. 2004, in American Institute of Physics Conference Series, Vol. 735, Bayesian Inference and Maximum Entropy Methods in Science and Engineering: 24th International Workshop on Bayesian Inference and Maximum Entropy Methods in Science and Engineering, ed. R. Fischer, R. Preuss, & U. V. Toussaint (AIP), 395–405, doi: [10.1063/1.1835238](https://doi.org/10.1063/1.1835238)

Skilling, J. 2006, Bayesian Analysis, 1, 833, doi: [10.1214/06-BA127](https://doi.org/10.1214/06-BA127)

Skumanich, A. 1972, ApJ, 171, 565, doi: [10.1086/151310](https://doi.org/10.1086/151310)

Soderblom, D. R., Duncan, D. K., & Johnson, D. R. H. 1991, ApJ, 375, 722, doi: [10.1086/170238](https://doi.org/10.1086/170238)

Souza dos Santos, P. V., Porto de Mello, G. F., Costa-Bhering, E., et al. 2024, MNRAS, 532, 563, doi: [10.1093/mnras/stae1532](https://doi.org/10.1093/mnras/stae1532)

Spada, F., & Lanzafame, A. C. 2020, A&A, 636, A76, doi: [10.1051/0004-6361/201936384](https://doi.org/10.1051/0004-6361/201936384)

Speagle, J. S. 2020, MNRAS, 493, 3132, doi: [10.1093/mnras/staa278](https://doi.org/10.1093/mnras/staa278)

van Saders, J. L., Ceillier, T., Metcalfe, T. S., et al. 2016, Nature, 529, 181, doi: [10.1038/nature16168](https://doi.org/10.1038/nature16168)

Vaughan, A. H., & Preston, G. W. 1980, PASP, 92, 385, doi: [10.1086/130683](https://doi.org/10.1086/130683)

Vaughan, A. H., Preston, G. W., & Wilson, O. C. 1978, PASP, 90, 267, doi: [10.1086/130324](https://doi.org/10.1086/130324)

Vidotto, A. A., Gregory, S. G., Jardine, M., et al. 2014, MNRAS, 441, 2361, doi: [10.1093/mnras/stu728](https://doi.org/10.1093/mnras/stu728)

Wang, J.-H., Xiang, M., Zhang, M., et al. 2025, ApJS, 280, 13, doi: [10.3847/1538-4365/aded16](https://doi.org/10.3847/1538-4365/aded16)

Xiang, M., Liu, X., Shi, J., et al. 2017, ApJS, 232, 2, doi: [10.3847/1538-4365/aa80e4](https://doi.org/10.3847/1538-4365/aa80e4)

Yang, H., Liu, J., Soria, R., et al. 2025, A&A, 699, A251, doi: [10.1051/0004-6361/202554379](https://doi.org/10.1051/0004-6361/202554379)

Ye, L., Bi, S., Zhang, J., et al. 2024, ApJS, 271, 19, doi: [10.3847/1538-4365/ad1eee](https://doi.org/10.3847/1538-4365/ad1eee)

Zhang, J., Zhao, J., Oswalt, T. D., et al. 2019, ApJ, 887, 84, doi: [10.3847/1538-4357/ab4efe](https://doi.org/10.3847/1538-4357/ab4efe)

APPENDIX

A. FITTING RESULTS

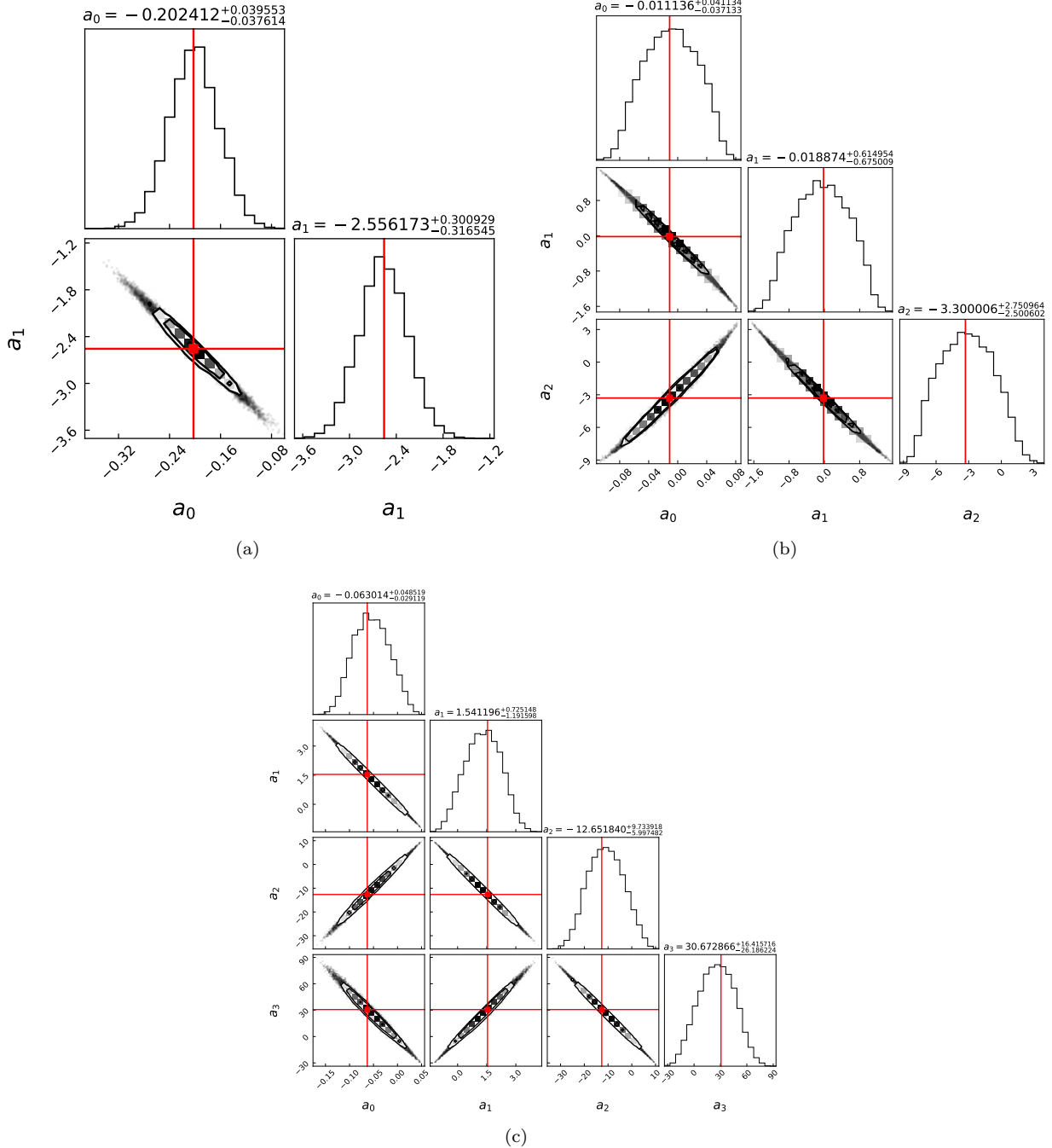


Figure A1. Examples of posterior probability distributions for the G-type star fits, using the standard deviation of $\log_{10}(R'_{\text{HK}})$ in each age bin as uncertainty. Panel (a), (b), and (c) represents 1st-, 2nd-, and 3rd-degree polynomial model, respectively.

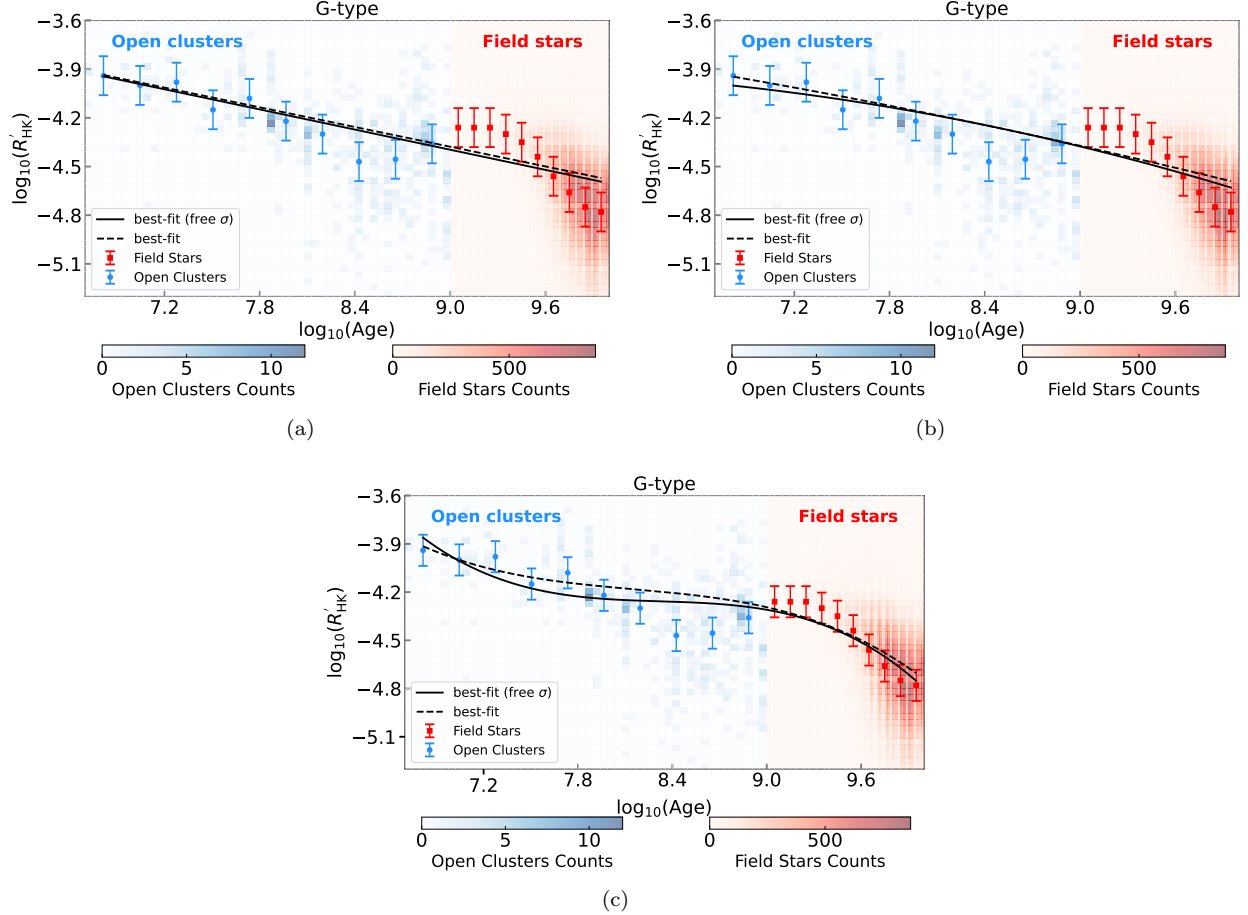


Figure A2. Comparison of R'_HK –age relations for G-type stars with different methods: fits using the standard deviation of $\log_{10}(R'_\text{HK})$ in each bin as the error (dashed lines), and fits with the error of $\log_{10}(R'_\text{HK})$ set as a free parameter (solid lines). Panels (a), (b), and (c) show the results for first-, second-, and third-order polynomial models, respectively.

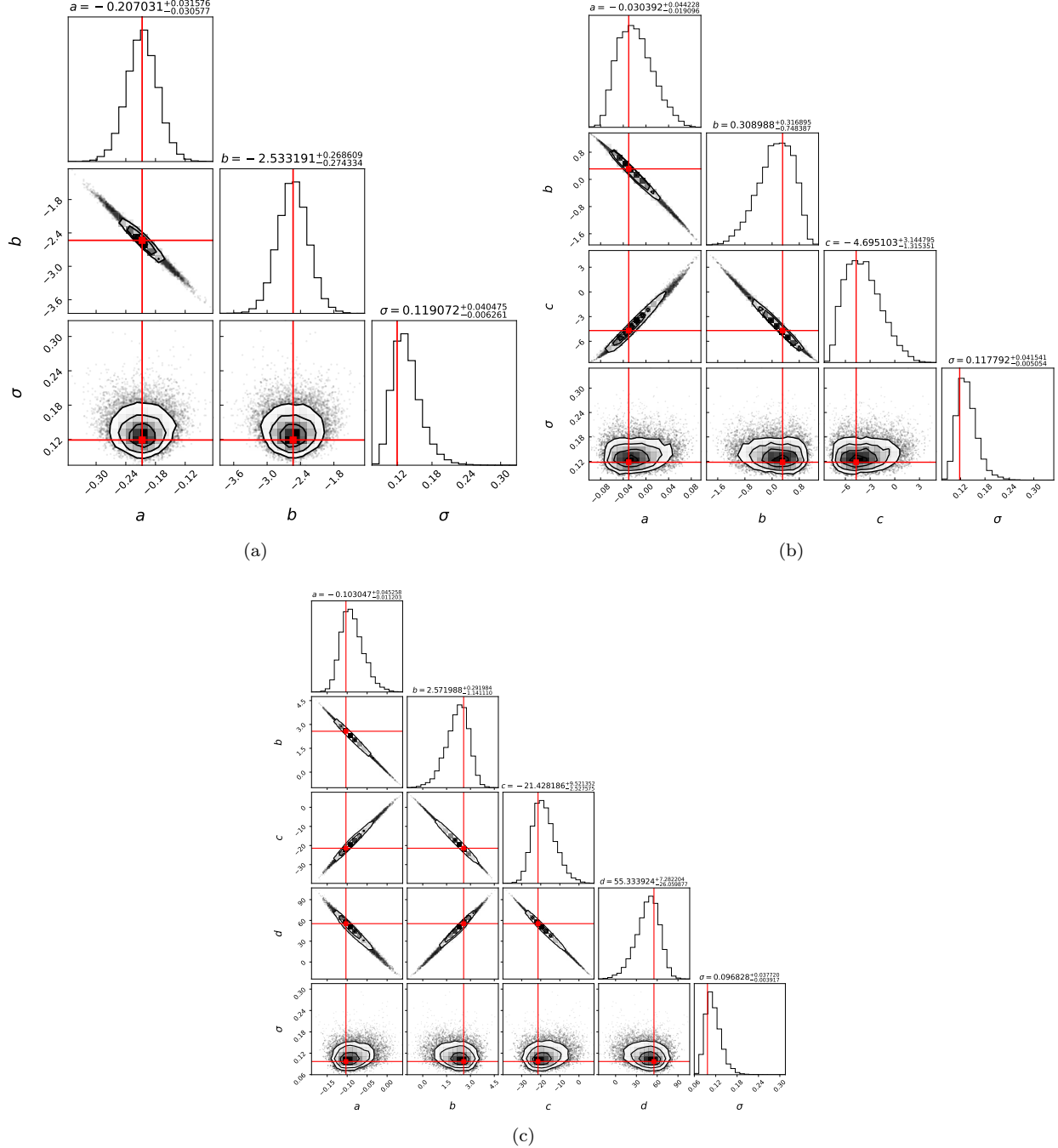


Figure A3. Posterior probability distributions for the G-type star fits, using σ as a free parameter. Panel (a), (b), and (c) represents 1st-, 2nd-, and 3rd-degree polynomial model, respectively.